Modified Hitschfeld–Bordan Equations for Attenuation-Corrected Radar Rain Reflectivity: Application to Nonuniform Beamfilling at Off-Nadir Incidence

ROBERT MENEGHINI

NASA Goddard Space Flight Center, Greenbelt, Maryland

LIANG LIAO

Goddard Earth Sciences and Technology Center, and Morgan State University, Greenbelt, Maryland

(Manuscript received 13 September 2012, in final form 14 December 2012)

ABSTRACT

As shown by Takahashi et al., multiple path attenuation estimates over the field of view of an airborne or spaceborne weather radar are feasible for off-nadir incidence angles. This follows from the fact that the surface reference technique, which provides path attenuation estimates, can be applied to each radar range gate that intersects the surface. This study builds on this result by showing that three of the modified Hitschfeld–Bordan estimates for the attenuation-corrected radar reflectivity factor can be generalized to the case where multiple path attenuation estimates are available, thereby providing a correction to the effects of nonuniform beamfilling. A simple simulation is presented showing some strengths and weaknesses of the approach.

1. Introduction

The nonuniform beamfilling problem for weather radars has attracted attention because it is a significant error source in estimating characteristics of the precipitation from space, such as in the Tropical Rainfall Measuring Mission (TRMM) precipitation radar (PR) (Kozu et al. 2001) and the dual-frequency precipitation radar (DPR) scheduled to be launched as part of the Global Precipitation Mission (GPM) satellite in early 2014. The field of view of the radars is approximately 5 km in diameter, so strong gradients in the radar reflectivity over the beam can be expected, particularly in convective storms. The problem is complicated by attenuation effects that make the problem global, in the sense that the measured radar return at any range depends not only on the local distribution of hydrometeors but also on the signal attenuation up to that range, which itself depends on the nonuniformity of the hydrometeor distribution along the path. When path attenuation is estimated by means of the surface return, the problem is further complicated by the fact that errors in this estimate depend on nonuniform beamfilling (NUBF) effects in a different way than for atmospheric targets. The NUBF surface effect can be understood most easily by imagining a nadir beam half filled with rain (Nakamura 1991); since the path attenuation estimate is obtained from the difference (in dB) of the surface return fully outside the rain with that in the rain (which in this case is assumed to be half filled), the estimate can never exceed 3 dB even when the rain rate, and therefore attenuation, in the filled portion is allowed to become arbitrarily large. It is worth noting that this example assumes a ray approximation, so that if half the beam is rain free and the other half filled with an arbitrarily large rain rate, the radar return from the surface will be approximately one-half that of the return from an entirely rain-free beam. The ray approximation will be used throughout the paper in computing path attenuation and measured radar reflectivity along individual ray paths within the beam.

By using a theoretical model of rain as well as high-resolution airborne data to simulate the TRMM PR geometry, Durden et al. (1998) showed explicitly how the NUBF affects estimates of path attenuation and attenuation-corrected radar reflectivity. Building on earlier work by Nakamura (1991) and Kozu and Iguchi (1996), Iguchi et al. (2000, 2009) showed that beamfilling

Corresponding author address: Robert Meneghini, NASA GSFC, Code 612, Greenbelt, MD 20771.
E-mail: robert.meneghini-1@nasa.gov

DOI: 10.1175/JTECH-D-12-00192.1

effects could be accounted for by a factor determined primarily by the coefficient of variation (the ratio of the standard deviation to the mean) of the attenuation coefficient. This simple and elegant result, however, comes at the expense of assuming range independence of the nonuniformity and restrictions on the form of the probability distribution of attenuation within the beam. More recently, Short et al. (2012) have shown simulation results, using measured ground-based radar data, indicating that useful corrections to the NUBF can be obtained from this formulation when some of the assumptions are relaxed.

The work here uses the results of Takahashi et al. (2006), who showed the feasibility of multiple estimates of path-integrated attenuation (PIA) over the field of view for an off-nadir geometry using data from the TRMM PR. Although their emphasis was on using the PIA variations across the beam to calculate a coefficient of variation to be used in the context of the Iguchi et al. (2000, 2009) NUBF formulation, the focus here is to use the multiple estimates of PIA to generalize some of the modified Hitschfeld–Bordan estimates, thereby addressing the NUBF problem via an analytic—rather than a statistical—formulation.

The basic radar geometry is shown in Fig. 1. The measured data are taken to be the low-resolution measured radar reflectivity factors, $\hat{Z}_{m,i}$, $(i = 1, \ldots, n)$ along each of the range gates (rows) and the estimated values of the path-integrated attenuation, A_j $(j = 1, \ldots, m)$ along the m columns. Note that the number of columns and their width are determined by the incidence angle, antenna beamwidth or field of view (FOV), and the range gate spacing. Each of the range gates that intersect the surface defines a sub-FOV column. By referencing the surface return at each of these gates to the surface return under rain-free conditions, an estimate of path attenuation can be obtained along each column. The shaded triangular region just above the surface, shown in Fig. 1, indicates the ranges where the surface return dominates the return from the precipitation, so that a measurement of the radar reflectivity factors at these gates is not possible. Indeed, to apply the surface reference technique (SRT) properly at these surface gates requires that the surface return be much larger than the rain return. In practice, the decision as to whether the surface or rain return dominates at a particular gate is not straightforward because it depends on the strength of the surface return, which in turn is a function of incidence angle, surface type, and rain intensity. In the treatment here, we will assume that this decision can be made without ambiguity.

The TRMM PR and GPM DPR radars are cross-track scanning instruments; that is, the scanning is orthogonal to the direction of the satellite motion, so that the schematic in Fig. 1 illustrates the off-nadir beam in the cross-track direction. In the along-track direction, there is no capability for enhanced resolution; nevertheless, as will be discussed later, for a dual-frequency radar, the procedure proposed by Tanelli et al. (2012) can provide information on the NUBF in the along-track direction.

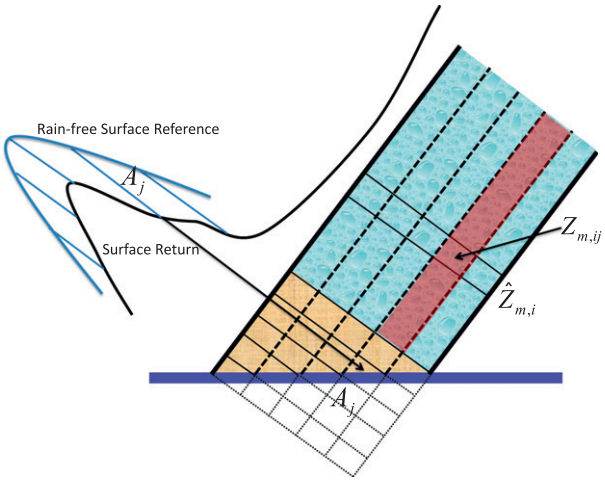

FIG. 1. Off-nadir cross-track geometry. The measured low-resolution radar reflectivity at range gate i is denoted by $\hat{Z}_{m,i}$, while the path-integrated attenuation along the jth column is denoted by A_j. The high-resolution measured radar reflectivity at the intersection of the ith range and jth column is denoted by $Z_{m,ij}$. (left) Determination of path attenuation, A_j, is illustrated as the difference in surface return powers along column j outside and inside the rain.

2. Modified Hitschfeld–Bordan equations

We can write down the Hitschfeld and Bordan (1954) (HB) equation for each of the $j = 1, \ldots, m$ columns for which a PIA estimate is available. These equations are expressed in terms of the high-resolution measured radar reflectivity factors. We use the term "measured" in the sense that the values are not corrected for attenuation; they are not measured in the sense that they can be derived from the radar return power. Only the coarse-resolution measured reflectivity factors can be derived from the radar return and radar equation. In writing the equations below, we follow the notation of Iguchi and Meneghini (1994).

The HB equation can be derived from the basic relationship between the measured reflectivity factor Z_m and attenuation-corrected radar reflectivity factor Z at range r as shown:

$$Z_m(r) = Z(r)10^{-0.2\int_0^r k(s)ds}, \tag{1}$$

where Z_m is directly proportional to the radar return power, and since the radar range and radar calibration

constant are assumed to be known, it can be considered a measured quantity. The quantity k is the specific attenuation in decibels per kilometer. Using a k–Z relation, $k = \alpha Z^{\beta}$, where α is allowed to vary with range but not β; substituting this into (1) and differentiating with respect to range gives a first-order differential equation, the solution of which, for the jth column, can be written as

$$Z_j(r) = Z_{m,j}(r)/[c - qS_j(r)]^{1/\beta}, \tag{2}$$

where $q = 0.2\beta \ln 10$, c is the constant of integration, and $S_j(r)$ is given by

$$S_j(r) = \int_0^r \alpha_j(s) Z_{m,j}^{\beta}(s)\, ds, \tag{3}$$

where the integration extends from the radar ($s = 0$) to an arbitrary range r ($s = r$). For the initial-value problem, $Z_j(0) = Z_{m,j}(0)$; since $S_j(0) = 0$, then $c = 1$, which gives the standard HB solution. It is worth noting that the C- and α-adjustment methods, described in sections 2a and 2b, respectively, begin with the initial-value (HB) solution and then modify either the calibration constant or α, so that the path attenuation from the HB solution is equal to that obtained from the surface reference method. For the final-value approach, described in section 2c, the constant of integration is determined by imposing a condition at the final range gate just above the surface. This condition is basically that the attenuation-corrected Z at the final range gate be equal to the measured Z at this same gate multiplied by an attenuation factor determined by the surface reference estimate.

To better understand the approximations that will be introduced, it is useful to express the HB solution, (2) with $c = 1$, along the jth column in terms of discrete range gates, where the first index gives the gate number and the second index the column number, as shown:

$$Z_{ij} = Z_{m,ij} \Big/ \left(1 - qh \sum_{k=1}^{i} \alpha_{kj} Z_{m,kj}^{\beta}\right)^{1/\beta}, \tag{4}$$

where h is the radar range resolution [to be more precise, a factor δ_{kj} should be introduced inside the summation to account for the fact that $\delta_{kj} = 1$ for $k \neq i$ and $\delta_{kj} \approx 0.5$ for $k = i$; to make the notation less cumbersome, this is omitted in (4) and subsequent equations]. Equation (4) states that the attenuation-corrected reflectivity factor at the ith range gate of the jth column is equal to the measured reflectivity factor at this same gate and column multiplied by a factor that depends on the parameters of the k–Z relationship and the measured high-resolution reflectivity factors in the column summed from the storm top to the ith range gate. Comparing (4) with (1) shows that this factor is closely related to the path attenuation from the storm top to the ith range gate. In particular, if we choose the range gate closest to the surface, $i = n_j$ or $r = r_s$, then we obtain the relationship

$$A_j^{\beta} \equiv 10^{-0.1\beta \mathrm{PIA}_j} \cong 1 - qh \sum_{i=1}^{n_j} \alpha_{ij} Z_{m,ij}^{\beta}, \tag{5}$$

where

$$\mathrm{PIA}_j = 2\int_0^{r_s} k_j(s)\, ds \approx 2h \sum_{i=1}^{n_j} k_{ij}. \tag{6}$$

The essence of the modification procedure is to replace the HB-derived attenuation factor [right-hand side of (5)] with that obtained from an independent estimate of this quantity, that is, the left-hand side of (6), where PIA_j is given by an independently measured value of PIA_j, which in our case is that provided by the surface returns within and outside the raining field of view. The difference in the present case is that the high-resolution quantity, $Z_{m,ij}$, is not measured, only the low-resolution quantity $\hat{Z}_{m,i}$, which is the beam-weighted average of the $Z_{m,ij}$ over the $j = 1, \ldots, m$ columns that comprise the radar field of view.

a. C adjustment

For the C- and α-adjustment procedures (Meneghini et al. 1983; Meneghini and Nakamura 1990), the $Z_{m,ij}$ or α_{ij} are modified by a multiplicative factor in a way that the HB estimate of attenuation is made equal to that from the surface reference technique. For the C-adjustment case, the following assumptions are made:

$$Z_{m,ij} = \varepsilon_j^{1/\beta} \hat{Z}_{m,i} \quad \text{and}$$
$$\alpha_{ij} = \alpha_i. \tag{7}$$

Note that the first equation of (7) is a twofold approximation: in the first, the high-resolution reflectivity factors are modified by $\varepsilon_j^{1/\beta}$; in the second, the high-resolution values are replaced by the low-resolution values. The variations in $Z_{m,ij}$ along each column can be thought of as being represented by the $\varepsilon_j^{1/\beta}$ term, while the variations in range can be thought of as being represented by the $\hat{Z}_{m,i}$ term so that, in effect, a separation of variables assumption is made. Substituting these relations into (5) and solving for ε_j gives

$$\varepsilon_j = (1 - A_j^\beta) \Big/ qh \sum_{i=1}^{n_j} \alpha_i \hat{Z}_{m,i}^\beta . \quad (8)$$

Substituting (7) and (8) into (4) gives an expression for the high-resolution attenuation-corrected radar reflectivity factors in terms of the measured values of path-attenuation and coarse-resolution measured radar reflectivity factors:

$$(Z_{ij})_C = \hat{Z}_{m,i} \varepsilon_j^{1/\beta} \Big/ \left(1 - qh\varepsilon_j \sum_{k=1}^{i} \alpha_k \hat{Z}_{m,k}^\beta\right)^{1/\beta} . \quad (9)$$

b. α adjustment

For the α-adjustment case, the following assumptions are used:

$$Z_{m,ij} = \hat{Z}_{m,i} \quad \text{and}$$
$$\alpha_{ij} = \varepsilon_j \alpha_i . \quad (10)$$

Substituting these relations into (5) and solving for ε_j gives the same result as (8). Substituting (10) and (8) into (4) gives the α-adjustment result for the attenuation-corrected high-resolution radar reflectivity at the ith gate and jth column as

$$(Z_{ij})_\alpha = \hat{Z}_{m,i} \Big/ \left(1 - qh\varepsilon_j \sum_{k=1}^{i} \alpha_k \hat{Z}_{m,k}^\beta\right)^{1/\beta} . \quad (11)$$

c. Final value

For the final-value analog, we return to the general solution given by (2) and write

$$Z_{ij} = Z_{m,ij} \Big/ \left(c - qh \sum_{k=1}^{i} \alpha_{kj} Z_{m,kj}^\beta\right)^{1/\beta} . \quad (12)$$

In this approximation, we assume

$$Z_{m,ij} = \hat{Z}_{m,i} \quad \text{and}$$
$$\alpha_{ij} = \alpha_i . \quad (13)$$

One way to derive the final-value formulation (Marzoug and Amayenc 1991, 1994) is to set the attenuation-corrected reflectivity at the last gate above the surface equal to the measured reflectivity factor multiplied by the attenuation factor derived from the SRT (Iguchi and Meneghini 1994). Again, letting the last gate of the jth column (that closest to the surface) be denoted by n_j, then

$$Z_{ij}(i = n_j) = Z_{m,ij}(i = n_j) \Big/ \left(c - qh \sum_{k=1}^{n_j} \alpha_{kj} Z_{m,kj}^\beta\right)^{1/\beta} ,$$
$$= Z_{m,ij}(i = n_j)/A_j = \hat{Z}_{m,i}(i = n_j)/A_j . \quad (14)$$

Note that (13) is used for the right-most equality in (14), where the measured high-resolution reflectivity at the n_j gate, jth column is set equal to the low-resolution value at gate n_j. Solving for c and using (13) gives

$$c = A_j^\beta + qh \sum_{i=1}^{n_j} \alpha_i \hat{Z}_{m,j}^\beta . \quad (15)$$

Substituting this into (12) and again using (13) yields the following expression for the high-resolution final-value radar reflectivity:

$$(Z_{ij})_{fv} = \hat{Z}_{m,i} \Big/ \left[A_j^\beta + qh\left(\sum_{k=1}^{n_j} \alpha_k \hat{Z}_{m,k}^\beta - \sum_{k=1}^{i} \alpha_k \hat{Z}_{m,k}^\beta\right)\right]^{1/\beta} . \quad (16)$$

d. Characteristics of the solutions

The HB modifications can be written in simpler forms by using a continuous range variable so that for column j ($j = 1, \ldots, m$),

$$[Z_j(r)]_C = \varepsilon_j^{1/\beta} \hat{Z}_m(r)/[1 - q\varepsilon_j \tilde{S}(r)]^{1/\beta} , \quad (17)$$

$$[Z_j(r)]_\alpha = \hat{Z}_m(r)/[1 - q\varepsilon_j \tilde{S}(r)]^{1/\beta} , \quad (18)$$

$$[Z_j(r)]_{fv} = \hat{Z}_m(r)/\{A_j^\beta + q[\tilde{S}(r_s) - \tilde{S}(r)]\}^{1/\beta} , \quad (19)$$

where $\tilde{S}$ *and* ε_j are given by

$$\tilde{S}(r) = \int_0^r \alpha(s) \hat{Z}_m^\beta(s)\, ds \quad \text{and} \quad (20)$$

$$\varepsilon_j = (1 - A_j^\beta)/q\tilde{S}(r_s) . \quad (21)$$

To calculate the attenuation-corrected reflectivity factor and rain rate over the low-resolution range gate, the antenna-gain-weighted sum of the high-resolution data is needed. Denoting the weight along the jth column by w_j, then the low-resolution attenuation-corrected radar reflectivity factor at the ith range gate can be expressed as

$$(Z_i)_{\text{method}} = \sum_{j=1}^{m} w_j (Z_{ij})_{\text{method}} \Big/ \sum_{j=1}^{m} w_j . \quad (22)$$

To obtain high-resolution rain rates, an R–Z ($R = aZ^b$) relationship is applied to the high-resolution Z data. We define the low-resolution rain rates by a formula similar to (22):

$$(R_i)_{\text{method}} = \sum_{j=1}^{m} w_j (aZ_{ij}^b)_{\text{method}} \Big/ \sum_{j=1}^{m} w_j, \qquad (23)$$

where "method" is used to represent the C-adjustment, α-adjustment, or final-value expression for the Z_{ij} estimates given by (9), (11), and (16), respectively. In the case of the α adjustment, it can be argued that a change in α implies a change in the parameters of the R–Z relationship, so that in this case, the a and b parameters in (23) would be replaced by a_j and b_j, respectively, tuned to the modified α value, that is, the initial value of α multiplied by ε_j.

The relative magnitudes of (17)–(19) are determined entirely by the magnitude of ε_j and follow directly from the results of Iguchi and Meneghini (1994) as follows:

$$\begin{aligned} &\text{if} \quad \varepsilon_j > 1 \quad \text{then} \quad [Z_j(r)]_C > [Z_j(r)]_{fv} > [Z_j(r)]_\alpha, \\ &\text{if} \quad \varepsilon_j = 1 \quad \text{then} \quad [Z_j(r)]_C = [Z_j(r)]_{fv} = [Z_j(r)]_\alpha, \\ &\text{if} \quad \varepsilon_j < 1 \quad \text{then} \quad [Z_j(r)]_C < [Z_j(r)]_{fv} < [Z_j(r)]_\alpha. \end{aligned} \qquad (24)$$

It is also worth noting that if the path attenuations in any two columns are equal, then the results for any of these methods will be the same for these two columns. For example, if the path attenuations along columns k and n are equal, then at any range

$$[Z_{j=k}(r)]_{\text{method}} = [Z_{j=n}(r)]_{\text{method}}, \qquad (25)$$

where "method" must be the same on both sides of this equation. However, if $\varepsilon_{j=k} = \varepsilon_{j=n} = 1$, then according to (24), all the methods will yield the same profile of the attenuation-corrected reflectivity in the two columns. When all m path attenuations are the same, the results reduce to the standard formulations, implying that uniform beamfilling conditions hold in the cross-track direction. Moreover, if all the path attenuations are the same and $\varepsilon = 1$, then all the HB-modified formulations reduce to the HB solution.

What we call the "NUBF" solutions for the low-resolution reflectivity factor and rain rate are given by (22) and (23), where the Z_{ij} are given by (9), (11), or (16). For the "non-NUBF" or traditional solutions, we take only a single estimate of the path attenuation, corresponding to a value that would be obtained near the nominal surface maximum, that is, the path attenuation estimate along the central column of the antenna beam. If we assume for convenience that the number of columns m is odd, then we define the center ray, j_c, equal to $(m + 1)/2$. In this case, the non-NUBF solutions are given by the above formulas using a single path attenuation at $j = j_c$, so that the summations in (22), (23) reduce to a single term at $j = j_c$. Note that the HB solution is inherently a low-resolution result, since it does not use any independent path attenuation information. Using (4) and (13) gives the traditional HB solution for the attenuation-corrected reflectivity factor at the ith range gate:

$$(Z_i)_{\text{HB}} = \hat{Z}_{m,i} \Big/ \left(1 - qh \sum_{k=1}^{i} \alpha_k \hat{Z}_{m,k}^{\beta}\right)^{1/\beta}. \qquad (26)$$

3. Simulation and results

Because of the wide variety of nonuniform beamfilling geometries and radar incidence angles, it is difficult to draw general conclusions on the degree of improvement of any NUBF correction procedure. The intention here is to identify some strengths and weaknesses of the approach and suggest possible directions for future work. An obvious weakness of the approach is that it provides no NUBF information in the along-track direction. Another potentially major limitation is that it assumes that multiple PIA estimates can be measured at off-nadir incidence angles. Apart from the inherent errors in the SRT itself (Meneghini et al. 2000, 2004; Seto and Iguchi 2007) are the potential error sources that can arise when the rain return (at the early surface gates, before the peak return) and bistatic and mirror-image returns (at later gates, after the peak) add to estimation errors. These error sources are neglected here but must be considered before any approach using multiple PIA estimates via the SRT can be fully validated. A related error source is the dynamic range: in many cases, the surface return will be detected along the central ray of the FOV but not at nearby range gates because of lower signal-to-noise ratios at the surface. In these cases, a restricted set of PIAs must be used in the retrievals.

In the simulation presented, we neglect biases and fluctuations in the measured radar reflectivity factors and assume that the k–Z relationship is exact; that is, the k–Z relationship used to generate the model data is the same as that used in the retrievals. As explained below, we also assume that the path attenuation estimates have no error if the reflectivity factors are uniform in the along-track direction. To evaluate the summations of $\hat{Z}_{m,i}$ that occur in the various formulations requires an assumption as to what these values should be in the triangular region near the surface shown in Fig. 1. As the $\hat{Z}_{m,i}$ are not

measurable in this region, because the surface is assumed to dominate the return power, we assume that the values of $\hat{Z}_{m,i}$ at range gates lower than the last nonclutter-dominated range gate are equal to the value measured at that range gate [if the attenuation-corrected Z_i rather than the $\hat{Z}_{m,i}$ were taken to be constant, then the HB equation itself could be used to estimate $\hat{Z}_{m,i}$ in the clutter region (Iguchi et al. 2009); for simplicity, we assume that the $\hat{Z}_{m,i}$, rather than the Z_i, values are constant in this region.] Labeling the gate at the storm top (first measureable gate) as 1 and the last nonclutter-dominated gate as i_s, this assumption is equivalent to $\hat{Z}_{m,i} = \hat{Z}_{m,i_s}; i > i_s$.

To construct a simple model storm, we begin by prescribing the true (nonattenuated) reflectivity factor (in dB) as a function of the Cartesian coordinates, (x, y, z) in the form

$$Z_{\mathrm{dB}}(x, y, z) = f(x)g(y)h(z), \tag{27}$$

where the functions on the right-hand side are taken to be linear functions of the coordinates, for example,

$$\begin{aligned} f(x) &= f_1; & x_1 \geq x \\ &= f_1 + (f_2 - f_1)(x - x_1)/(x_2 - x_1); & x_1 < x < x_2 \\ &= f_2; & x_2 \leq x. \end{aligned} \tag{28}$$

In other words, the variation in Z_{dB} along the x direction is constant (f_1) for $x \leq x1$, then changes linearly from f_1 to f_2 as x goes from x_1 to x_2, and then is constant (f_2) for $x \geq x2$. Variations in y and z are specified in a similar manner. We take the x axis to be in the cross-track direction, y in the along-track direction, and z in the vertical. As in Fig. 1, the beam tilt is in the positive x direction (i.e., $\varphi = 0°$, where φ is the azimuthal angle in the x–y plane). Recall that the NUBF formulation can potentially correct for gradients in x and z but not in y.

The radar geometry is defined by the incidence angle with respect to nadir, the 3-dB beamwidth (or field of view), and the range gate spacing. The radar frequency is taken to be that of the TRMM PR where $f = 13.8$ GHz. For an incidence angle of 15°, and a 0.71° beamwidth from an altitude of 400 km and a gate spacing of 125 m, we obtain approximately 11 range gates that intersect the surface; for an incidence angle of 10°, the number of surface gates reduces to 7; for 5°, the number decreases to about 3. In the results to be presented, the incidence angle is fixed at 10° but the results remain qualitatively the same at 15°. The radar beam is positioned so that its center at the surface ($z = 0$) is at $x = y = 0$. As this, along with the incidence angle and gate spacing, defines the high-resolution radar grid (see Fig. 1), the $Z(x, y, z)$ can be resampled onto the radar coordinates. The medium is assumed to consist only of rain, so that a single k–Z relationship can be used to generate the k field at each of the high-resolution grid points. From k and Z, we can compute Z_m at each high-resolution grid point by summing the path attenuations along ray paths from the storm top to the (i, j) grid point. Extending the ray path to the surface gives the total path attenuation along the ray. The low-resolution Z_m and Z are derived from the high-resolution data by weighting them by the antenna gain function, which is assumed to be a Gaussian with a (two ways) 6-dB beamwidth of 0.71°.

The path attenuation for the jth column, as derived by the SRT, is computed in the following way: assume that the jth column consists of k_m rays in the along-track direction, where the path attenuation along each of the rays is denoted by PIA_{jk}; $k = 1, \ldots, k_m$; and also assume that the intrinsic (not including atmospheric attenuation) normalized surface cross sections (NRCS) at the termination of these rays are all equal to $\sigma_R^0(\theta)$, where the subscript R indicates that the measurement is made in rain at an incidence angle, θ. The SRT estimate of total path attenuation along the jth column can be written as

$$\begin{aligned} \mathrm{PIA}_j &= 2\int_0^{r_s} k_j(s)\,ds \\ &= 10\log_{10}\left[\sigma_{NR}^0(\theta)\sum_{k=1}^{k_m} w_{jk} \Big/ \sigma_R^0(\theta)\sum_{k=1}^{k_m} w_{jk}10^{-0.1\mathrm{PIA}_{jk}}\right], \end{aligned} \tag{29}$$

where the numerator and denominator are proportional to the surface return power outside and inside the rain, respectively; and where w_{jk} are the antenna gain weighting factors and $\sigma_{NR}^0(\theta)$ is the NRCS in the rain-free area. If $\mathrm{PIA}_{jk} = \mathrm{PIA}_j$ for $k = 1, \ldots, k_m$ and if the intrinsic values of the normalized surface cross section are the same outside and inside the rain [$\sigma_{NR}^0(\theta) = \sigma_R^0(\theta)$], then the estimated PIA_j reduces to the true value. Note that the first assumption ($\mathrm{PIA}_{jk} = \mathrm{PIA}_j$ for $k = 1, \ldots, k_m$) implies uniform beamfilling in the along-track direction over the jth column; the second assumption, $\sigma_{NR}^0(\theta) = \sigma_R^0(\theta)$, takes the intrinsic surface cross sections to be the same inside and outside the rain. For the results to be presented, the latter assumption will always be taken to be valid; consequently, if there are no variations in Z in the along-track direction, then measured path attenuations will be equal to the true values. It is worth noting that the true PIA can be defined as 10 $\log_{10}$ of the ratio of the attenuation-corrected Z to the measured Z along the jth column so that, with the notation above,

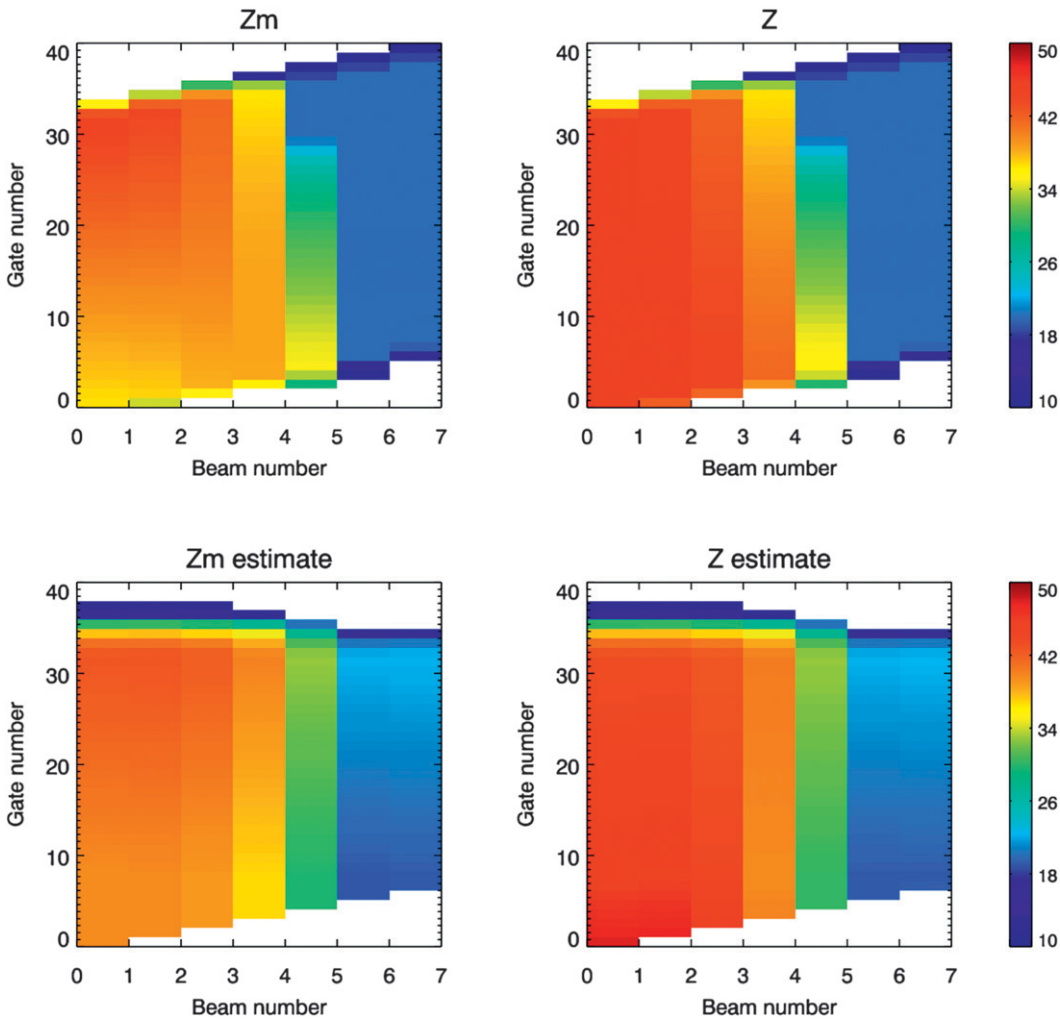

FIG. 2. (top) High-resolution true/input values of Z_m and Z for an incidence angle of 10° assuming Z changes linearly (dB) along the x axis (cross-track direction) from 45 to 20 dBZ in going from $x = -1$ km to $x = 1$ km, where the center of the beam at the surface is at $x = 0$, $y = 0$. (bottom) High-resolution estimates of Z_m and Z using the C-adjustment approach [Eqs. (7)–(9)].

$$\mathrm{PIA}_{j,\mathrm{True}} = 10\log_{10}\left(\sum_{k=1}^{k_m} w_{jk}Z_{jk} \Big/ \sum_{k=1}^{k_m} w_{jk}Z_{jk}10^{-0.1\mathrm{PIA}_{jk}}\right),$$

where Z_{jk} is to be interpreted as the attenuation-corrected Z at the termination of the path in the kth along-track segment of the jth cross-track column. If $Z_{jk} = Z_j$ for all k and if $\sigma^0_{NR}(\theta) = \sigma^0_R(\theta)$, then the above equation and (29) are identical.

Shown in the top plots of Fig. 2 are the high-resolution input Z_m and Z fields for an incidence angle of 10°, a storm height of 4 km, and a range gate of 125 m. Note that the data are plotted with the range gate number along the ordinate and the column number along the abscissa. Under these assumptions, the total number of gates that are partially or fully filled with rain is 40; however, the last seven gates (equal to the number of columns) correspond to the shaded near-surface region shown in Fig. 1. The radar-measured data are assumed to be the 33 values of the low-resolution $\hat{Z}_{m,i}$ above the surface as obtained from the weighted average of the high-resolution data, $Z_{m,ij}$. We also assume that measurements of the PIA along the seven columns are available. For the NUBF correction, the C-adjustment formulas given by (7)–(9) are used because, for the cases considered, these formulas yielded somewhat more accurate results than the other two. Although the reason for this behavior is not fully understood, the NUBF effect appears to be similar to a calibration error in Z so that the C-adjustment method, which modifies Z_m, is

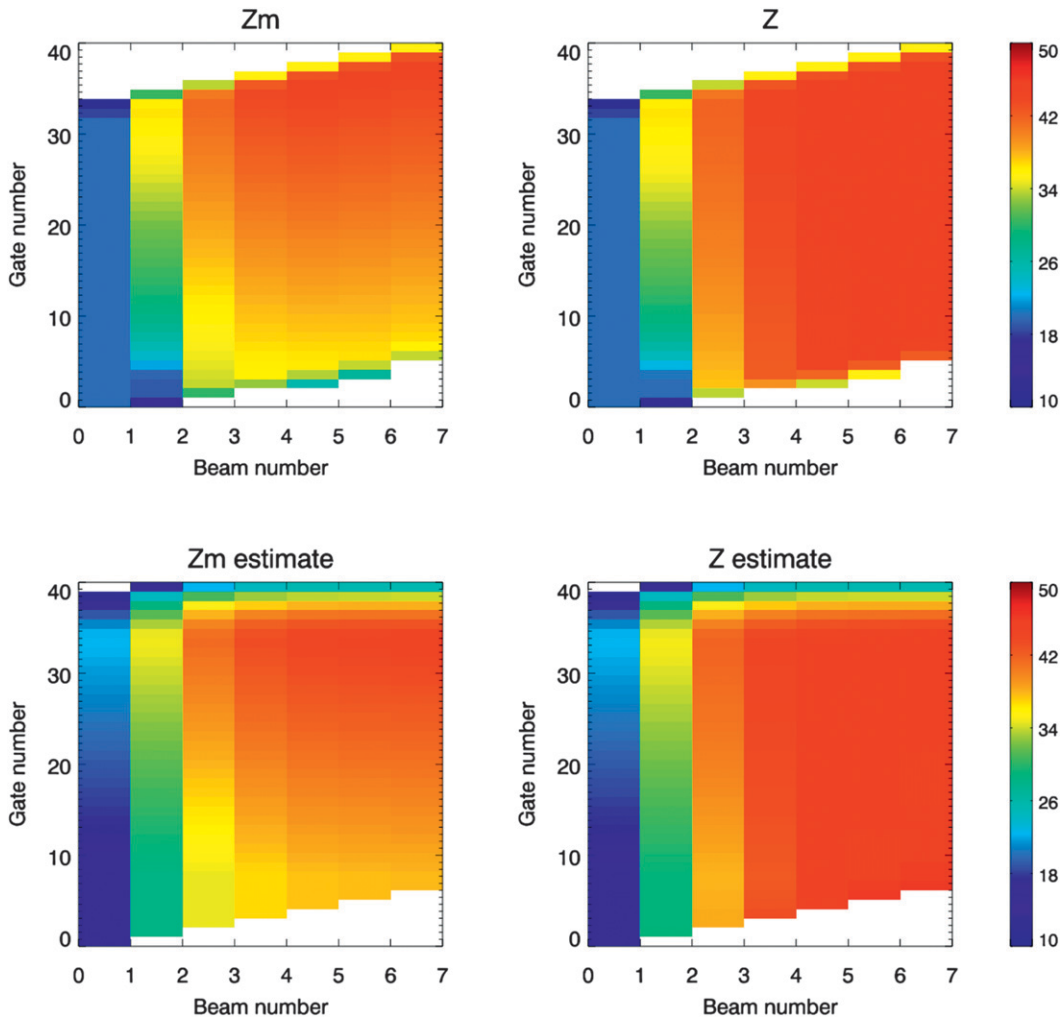

FIG. 3. (top) High-resolution true/input values of Z_m and Z for an incidence angle of 10° assuming Z changes along the x axis (cross-track direction) from 20 to 45 dBZ in going from $x = -1$ km to $x = 1$ km. (bottom) High-resolution estimates of Z_m and Z using the C-adjustment approach [Eqs. (7)–(9)].

most effective in minimizing the error. It should be emphasized, however, that the final-value and α-adjustment formulations should be considered when doing an analysis where the NUBF effect is not the only source of error.

Using (7)–(9) gives the estimated Z_m and Z high-resolution fields shown in the bottom two panels. In generating these results, we have assumed that the true or input Z has a negative gradient along x, going from 45 to 20 dBZ when x changes from -1 to 1 km. Recall that the diameter of the FOV is approximately 5 km. A second example is shown in Fig. 3, where the sign of the gradient is reversed so that Z changes from 20 to 45 dBZ when x increases from -1 to 1 km.

The low-resolution results for these two cases, obtained from (22) and (23), are shown in Fig. 4, where the left-hand pair of plots for Z and R is derived from the negative x-gradient case of Fig. 2 and the right-hand pair of plots is derived from the positive x-gradient case of Fig. 3. Note that the true or input values are represented by the solid lines and that the NUBF correction results, from the C-adjustment method, are represented by the dotted lines. For comparison purposes, the standard results from the HB, C-, and α-adjustment methods are also shown. To reduce the number of lines, the standard final-value results are not displayed but they fall between the standard C- and α-adjustment results. As seen in the results in Fig. 4, the NUBF-corrected values of Z and R are closer to the true values than are the traditional non-NUBF results, both in magnitude and shape of the range profile. Although the standard α-adjustment result for Z in the top-right-hand plot of Fig. 4 is quite close to the true Z profile, the corresponding R estimate in the bottom right shows an overestimation.

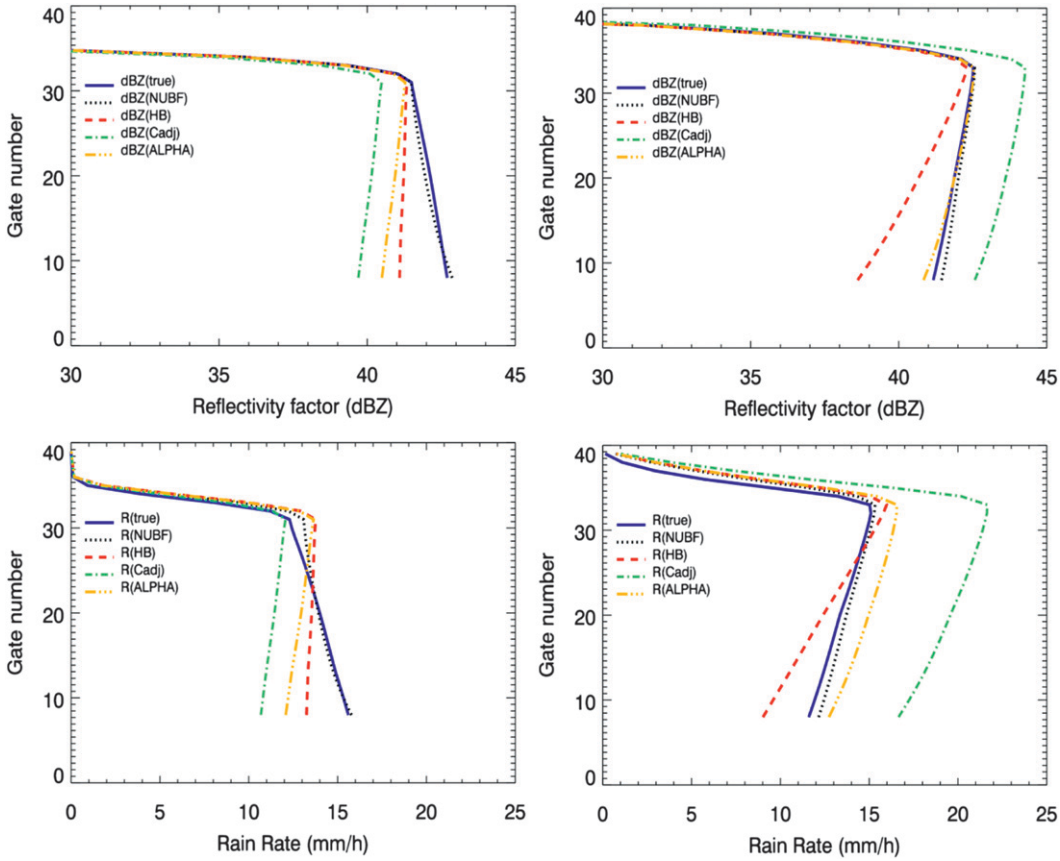

FIG. 4. Low-resolution estimates of Z and R, Z(NUBF), and R(NUBF), represented by the dotted lines, derived from the high-resolution estimates of Z shown in bottom-right panel of Fig. 2. True Z and R are represented by the solid lines. Also shown are the results from the low-resolution standard HB, C-adjustment, and α-adjustment formulations. (left) Results for a negative gradient in x, where $Z_{\mathrm{dB}}(x = -1) = 45$, $Z_{\mathrm{dB}}(x = 1) = 20$; (right) results for a positive gradient in x, where $Z_{\mathrm{dB}}(x = -1) = 20$, $Z_{\mathrm{dB}}(x = 1) = 45$.

A second set of results is shown in Fig. 5. For these cases, a positive gradient in $Z(x)$ from 20 to 45 dBZ is assumed but the location of the gradient is changed from the previous cases. For the left-hand plots, the gradient in the cross-track plane is taken over the range $(-2$ km, $0)$, while for the right-hand plots the gradient is taken over the range $(0, 2$ km$)$. For both cases and for both Z and R, the NUBF results are slightly higher than the true values but provide more accurate shapes and amplitudes than the standard non-NUBF results.

Examples that show the effects of gradients in both x and z are shown in Fig. 6. For these examples, $Z_{\mathrm{dB}}(x)$ is assumed to have a negative gradient, going from 45 dBZ at $x = -1$ km to 20 dBZ at $x = 1$ km. For the left-hand plots of Z and R, a positive gradient in z is assumed, so that $Z_{\mathrm{dB}}(z)$ is decreased from its nominal value by 3 dB at the surface and increased from its nominal value by 3 dB at the storm top (4 km). For the right-hand plots, the opposite is assumed, so that $Z_{\mathrm{dB}}(x, z)$ has a negative 6-dB gradient along the vertical. In contrast to the previous example, the NUBF results are usually a bit lower than the true values; but like the previous examples, they follow closely the true Z and R profiles.

Other examples, not shown, were used to confirm the fact that all the methods converge to approximately the same Z and R results in the absences of any gradients. In these cases, the values of PIA along the columns are equal and the corresponding epsilon values are approximately equal to 1. Two points are worth noting, however. The first point is the fact that all PIAs are equal implies only that the epsilons are equal, not that they are equal to one. For epsilon to be one, the HB and SRT estimates of PIA need to agree or be biased by the same amount. The former case applies for the results here because the k–Z relationship is taken to be exact and the PIA estimates are taken to be equal to the true values. The second point is that although errors occur because of the constant Z_m assumption in the nonobserved portion of the beam (the triangular region shown in Fig. 1), the retrieval results are nevertheless fairly close to the true values.

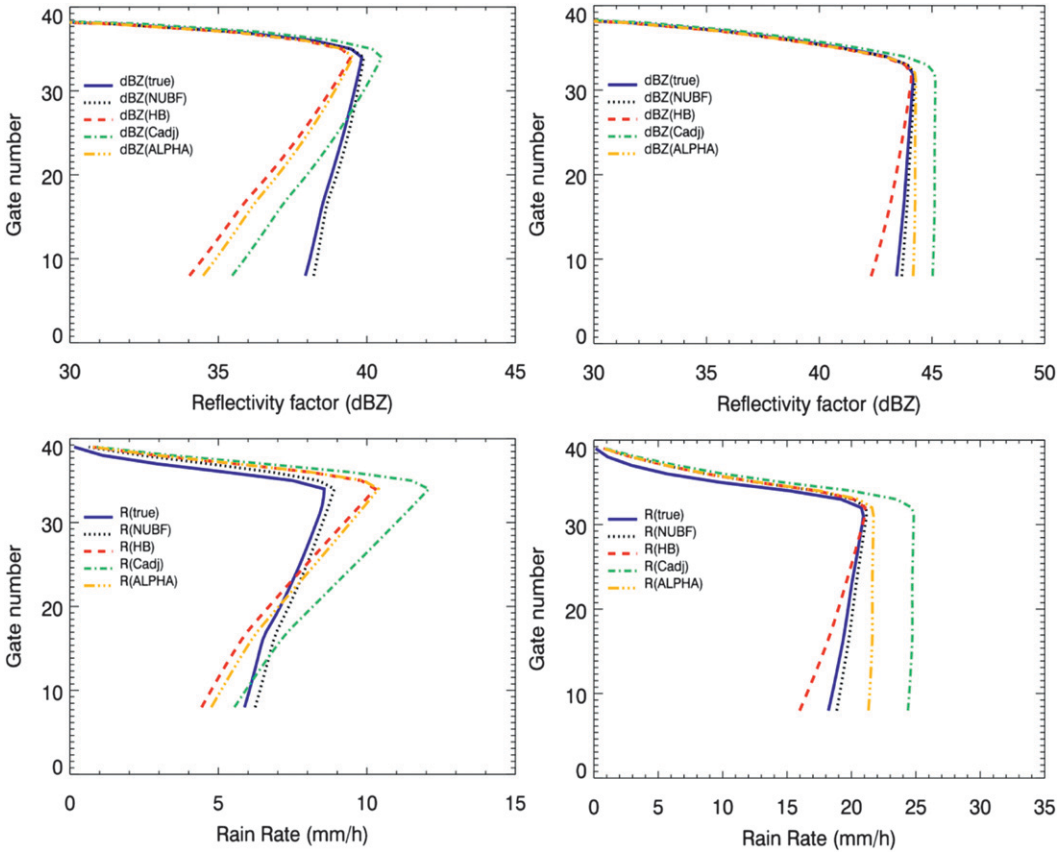

FIG. 5. Low-resolution estimates of Z and R, Z(NUBF), and R(NUBF), represented by the dotted lines. True Z and R are represented by the solid lines. Also shown are the results from the low-resolution standard HB, C-adjustment, and α-adjustment formulations. (left) Positive gradient in Z_{dB} along the x axis, where $Z_{dB}(x = 0) = 20$ and $Z_{dB}(x = 2) = 45$; (right) positive gradient in Z_{dB} along the x axis, where $Z_{dB}(x = -2) = 20$ and $Z_{dB}(x = 0) = 45$.

Examples with gradients only in the along-track direction show, as expected, that the NUBF corrections discussed here provide no improvement over the standard attenuation correction formulations. It is worth pointing out, however, that in a dual-frequency matched-beam case, such as the proposed dual-frequency spaceborne weather radar for the GPM mission where dual-frequency data will be available from nadir to about 9°, the procedure described by Tanelli et al. (2012) (see also Durden and Tanelli 2008) will be applicable. The authors argue that under uniform beamfilling conditions, the ratio of the Ka-band to Ku-band path attenuations will be approximately equal to the nominal theoretical value; under nonuniform conditions, the attenuation ratio will tend toward smaller values, since the limiting value of the PIA will be determined by the fraction of the beam filled with lower values of reflectivity and attenuation. In the ideal case where the cross-track estimates of PIA from the Ka-band and Ku-band channels all have a ratio close to the theoretical value, the indication would be of minimal nonuniformity in the along-track direction, allowing an application of one of the NUBF formulas above to correct for cross-track nonuniformity. However, the formulas above apply to a single-frequency radar; whether dual-frequency retrieval methods can be generalized in a similar way when multiple estimates of the PIA are available is an open but important question.

As a final comment, it is worth mentioning that with $(n + m)$ measurements (n measurements of Z_m and m measurements of PIA) but approximately $n \times m$ unknowns (the high-resolution attenuation-corrected radar reflectivity factors), there are many potential solutions to the problem other than those presented here. Whether alternative methods of solution can be devised and whether these solutions can provide more accurate results than those given here are open issues.

4. Summary

Multiple estimates of path attenuation over the cross-track beam at off-nadir incidence angles can be used to generalize some of the traditional attenuation correction

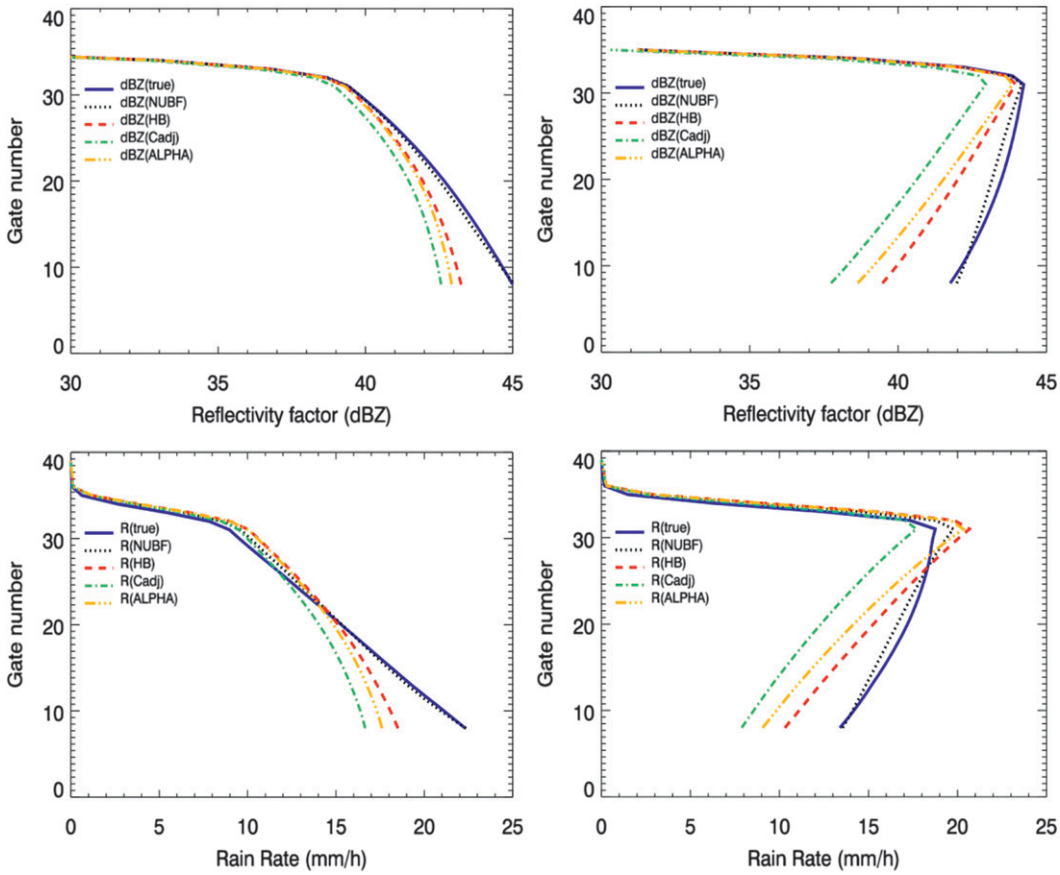

FIG. 6. Retrieval results for Z and R for an input Z field with a linear (dB) negative gradient along the x axis [$Z_{dB}(x = -1) = 45$, $Z_{dB}(x = 1) = 20$] multiplied by a linear (dB) 6-dB gradient in z over the 4-km storm height. (left) Negative gradient in Z_{dB} along the vertical (decreasing with height); (right) positive gradient in Z_{dB} along the vertical (increasing with height). True values are represented by the solid lines and NUBF-corrected results by the dotted lines. Also shown are the standard results from the HB, α-adjustment, and C-adjustment methods.

methods that have been used for airborne and spaceborne weather radars. A simple simulation used to test the modified formulations shows that the attenuation correction procedures work well with linear gradients in Z_{dB} in the cross-track plane. Future work will focus on an application of these results to airborne and spaceborne weather radar data and to possible extensions to dual-frequency radars.

Acknowledgments. This work is supported by Dr. Ramesh Kakar of NASA headquarters under NASA's Precipitation Measurement Mission Program NNH09ZDA001N-PRECIP.

REFERENCES

Durden, S. L., and S. Tanelli, 2008: Predicted effects of nonuniform beam filling on GPM radar data. *IEEE Geosci. Remote Sens. Lett.,* **5,** 308–310.

——, Z. S. Haddad, A. Kitiyakara, and F. K. Li, 1998: Effects of nonuniform beam filling on rainfall retrieval for the TRMM precipitation radar. *J. Atmos. Oceanic Technol.,* **15,** 635–646.

Hitschfeld, W., and J. Bordan, 1954: Errors inherent in the radar measurement of rainfall at attenuating wavelengths. *J. Meteor.,* **11,** 58–67.

Iguchi, T., and R. Meneghini, 1994: Intercomparison of single-frequency methods for retrieving a vertical rain profile from airborne or spaceborne radar data. *J. Atmos. Oceanic Technol.,* **11,** 1507–1516.

——, T. Kozu, R. Meneghini, J. Awaka, and K. Okamoto, 2000: Rain profiling algorithm for the TRMM precipitation radar. *J. Appl. Meteor.,* **39,** 2038–2052.

——, ——, J. Kwiatkowski, R. Meneghini, J. Awaka, and K. Okamoto, 2009: Uncertainties in the rain profiling algorithm for the TRMM precipitation radar. *J. Meteor. Soc. Japan,* **87A,** 1–30.

Kozu, T., and T. Iguchi, 1996: A preliminary study of non-uniform beam filling correction for spaceborne radar rainfall measurement. *IEICE Trans. Commun.,* E79-B, 763–769.

——, and Coauthors, 2001: Development of precipitation radar onboard the Tropical Rainfall Measuring Mission (TRMM) satellite. *IEEE Trans. Geosci. Remote Sens.,* **31,** 102–116.

Marzoug, M., and P. Amayenc, 1991: Improved range-profiling algorithm of rainfall rate from a spaceborne radar with path-integrated attenuation constraint. *IEEE Trans. Geosci. Remote Sens.,* **29,** 584–592.

——, and ——, 1994: A class of single-and dual-frequency algorithms for rain-rate profiling from a spaceborne radar. Part I: Principle and tests from numerical simulations. *J. Atmos. Oceanic Technol.,* **11,** 1480–1506.

Meneghini, R., and K. Nakamura, 1990: Range profiling of the rain rate by an airborne weather radar. *Remote Sens. Environ.,* **31,** 193–209.

——, J. Eckerman, and D. Atlas, 1983: Determination of rain rate from a space-borne radar using measurements of total attenuation. *IEEE Trans. Geosci. Remote Sens.,* **21,** 34–43.

——, T. Iguchi, T. Kozu, L. Liao, K. Okamoto, J. A. Jones, and J. Kwiatkowski, 2000: Use of the surface reference technique for path attenuation estimates from the TRMM precipitation radar. *J. Appl. Meteor.,* **39,** 2053–2070.

——, J. A. Jones, T. Iguchi, K. Okamoto, and J. Kwiatkowski, 2004: A hybrid surface reference technique and its application to the TRMM precipitation radar. *J. Atmos. Oceanic Technol.,* **21,** 1645–1658.

Nakamura, K., 1991: Biases of rain retrieval algorithms for spaceborne radar caused by nonuniformity of rain. *J. Atmos. Oceanic Technol.,* **8,** 363–373.

Seto, S., and T. Iguchi, 2007: Rainfall-induced changes in actual surface backscattering cross sections and effects on rain estimates by spaceborne precipitation radar. *J. Atmos. Oceanic Technol.,* **24,** 1693–1709.

Short, D., K. Nakagawa, and T. Iguchi, 2012: Empirical test of theoretically based correction for path integrated attenuation in simulated spaceborne precipitation radar observations. *IEEE J. Sel. Top. Appl. Earth Obs. Remote Sens.,* **5,** 930–935.

Takahashi, N., H. Hanado, and T. Iguchi, 2006: Estimation of path-integrated attenuation and its nonuniformity from TRMM/PR range profile data. *IEEE Trans. Geosci. Remote Sens.,* **44,** 3276–3283.

Tanelli, S., G. F. Sacco, S. L. Durden, and Z. S. Haddad, 2012: Impact of non-uniform beam filling on spaceborne cloud and precipitation radar retrieval algorithms. *Remote Sensing of the Atmosphere, Clouds, and Precipitation IV,* T. Hayasaka, K. Nakamura, and E. Im, Eds., International Society for Optical Engineering (SPIE Proceedings, Vol. 8523), 852308, doi:10.1117/12.977375.